Thermal-Pressure-Driven Gas Flows through Micro Channels

2012 J. Phys.: Conf. Ser. 362 012045

(http://iopscience.iop.org/1742-6596/362/1/012045)

Thermal-Pressure-Driven Gas Flows through Micro Channels

Hassan Akhlaghi Akhlaghi[1], Ehsan Roohi

Department of Mechanical Engineering, Ferdowsi University of Mashhad, P.O. Box 91775-1111, Mashhad, Iran

E-mail: akhlaghi@alum.sharif.edu

Abstract. In this paper we study mass flow rate of rarefied gas flow through micro/nanoscale channels under simultaneous thermal and pressure gradients using an improved direct simulation Monte Carlo (DSMC) method. Before targeting thermal/pressure driven flows, we first analyze pressure-driven flows and verify our DSMC solver. Next, we study micro-/ nanochannels flows under simultaneous pressure-temperature gradients while our main objective is to predict mass flow rate increment due to thermal creep effects. The effects of thermal creep are studied over a wide range of flow rarefaction from the slip to free molecular regime. Our results showed that the non-dimensional thermal creep mass flow rate increments of the Poiseuille flow increases and approaches the value of 0.578 at free molecular limit.

1. Introduction

With the fast progress in micro/nanoscale devices and components, it is desired to obtain fundamental understanding of the transport phenomena in these devices. Additionally, a true understanding of the hydrodynamics and thermal physics of rarefied gas flows is crucial in design, fabrication, and operation of micro/nano-electro-mechanical-systems (MEMS/NEMS) [1-2]. Once the gas flow rarefies, the Knudsen number, defined as the ratio of gas mean free path to the characteristic length of the geometry, $\mathrm{Kn} = \lambda / \mathrm{H}$, increases and the flow analysis should be performed using accurate approaches based on the solution of the Boltzmann equation [3]. Discrete molecular modeling of direct simulation Monte Carlo (DSMC) is a key tool to model flow field in all degrees of rarefaction for both of mono/diatomic gases [4]. In DSMC, the gas is modeled as a collection of moving particles which interact through collisions. DSMC is known as one of the most successful particle simulation methods in analyzing the rarefied gaseous flows.

Literature survey shows that there are continuing attempts for mass flow prediction of pressure-driven and thermal-driven rarefied gas flows through micro-/nanoscale channels. In the case of pressure-driven flows through micro-/nanochannels, there are a wide set of analytical predictions for mass flow rate based on different wall velocity slip boundary conditions. In addition to pressure gradient, wall temperature gradient may generate mass flow rate at micro/nano scale. Thermal creep flows in gases occurs by non-uniform temperature distributions in the flow boundaries [5]. In this situation, fluid starts creeping from the cold region towards the hot one. Knudsen pumps, which operate based on thermal creep/transpiration flow due to non-uniform wall temperature distribution, are employed in MEMS/NEMS [6-9]. Thermal creep/transpiration problem is investigated by several authors using kinetic models of the Boltzmann equation. The flow between two parallel plates, where

[1] Corresponding author.

a constant unidirectional temperature gradient is applied to the plates, is a common flow configuration which is used in kinetic approaches. Loyalka *et al.* [10-14] presented kinetic theory analysis of thermal transpiration and mechanocaloric effects. They presented a general kinetic theory analysis and showed that the cross phenomena of thermal transpiration and mechanocaloric effect can be treated by the use of the variational technique for all rarefactions regimes. Kanki and Iuchi [15] investigated Poiseuille flow and thermal creep of a rarefied gas between two parallel plates using the (Bhatnagar-Gross-Krook) BGK model. They showed that the ratio of the flow rate of the thermal creep to that of the Poiseuille flow reduces to zero at the continuum flow limit and approaches to 0.5 as the density of the gas approaches to zero. Ohwada *et al.* [16] studied the Poiseuille and thermal transpiration flows of a rarefied gas between two parallel plates on the basis of the linearized Boltzmann equation for hard-sphere molecules. They predicted the mass fluxes of the Poiseuille and the thermal transpiration flows for the whole range of the Knudsen number with good accuracy compared to the existing numerical method and experimental results. They showed that in spite of Poiseuille flow, mass flux increase continuously in thermal transpiration flow versus the Knudsen number. Alexeenko *et al.* [7] numerically investigated the temperature driven gas flows in a two-dimensional finite length microchannel and a cylindrical tube using DSMC method, a discrete ordinate method for the ellipsoidal statistical model, and BGK model. They used a short channel with the length-to-height ratio of 5, pressure ratio equal to one and Knudsen number equal to 0.2. They generated creep effects with different wall temperature distributions. Their results showed that despite of the same inlet/outlet pressure values, there are pressure changes along the channel. They also examined the effects of various wall temperature distributions and compared different numerical methods. Taheri and Struchtrup [17] applied a streamwise constant temperature gradient over the walls of a microchannel and studied rarefied gas flow through the channel using fully linearized and semi-linearized forms of the regularized 13-moment (R13) equations.

Simultaneous thermally/pressure driven flows may be considered to control mass and energy flow rates in micro/nanochannels [17]. This physics is also employed in Knudsen pumps, as discussed before. Micro/nanoscale Knudsen pumps are essential for the realization of completely miniaturized devices such as gas sensors, fuel cells, and lab-on-a-chip systems [9]. Consequently, study of this class of micro/nano flows would be crucial for accurate design of MEMS/NEMS. However, there is not an archival study in the mass flow rate prediction of the Poiseuille flow under simultaneous thermal and pressure gradients. Therefore, the main objective of the current study is the mass flow rate prediction of the rarefied gas flow through micro/nanoscale channels under both thermal and pressure gradients over a wide range of Knudsen numbers. We use DSMC method as our direct simulation strategy.

2. DSMC Method

DSMC is a numerical tool to solve the Boltzmann equation based on the direct statistical simulation of the molecular processes described by the kinetic theory [4]. The primary principle of DSMC is decoupling of the motion and collision for all simulated particles. DSMC is considered as a particle method in which one particle represents a large bulk of real gas molecules. After fulfilling all molecular movements, the collisions between molecules are simulated in each cell separately. To simulate complex flow effectively, improvements in the basic DSMC algorithm has been recently suggested by Gallis *et al.* [18] and Stefanov [19, 20]. However, in the current work, we extend and optimize DSMC codes employed by Roohi and coworkers for simulation of different micro/nano flows [21-27]. The variable hard sphere (VHS) model is applied as our collision model in all simulations. We use the diffuse reflection model at the solid walls. In diffuse reflection, the emission of impinging molecules is not correlated with the pre-impingement state of the molecules. The outgoing velocity of molecules is randomly assigned according to a half-range Maxwellian distribution determined by the wall temperature. Full thermal and momentum accommodation coefficients are considered for the walls.

For a 2-D pressure driven flow, the values of pressure and temperature at the inlet and outlet and the value of pressure at the outlet should be specified. However, DSMC calculation does not use pressure magnitude directly. On the other hand, density and velocity at the inlet and outlet and temperature at the outlet are unknown while they are required for the DSMC simulation. For example, inlet and outlet density and velocity are required to calculate the number of particles injected into the flow field or the outlet temperature is required for calculation of the most probable speed of particles [4]. Benefiting from the characteristics theory, specified inlet/outlet pressure boundary conditions are implemented implicitly into the flow field through correcting density ρ and velocity U values [28, 29]. For a backward-running wave, we consider

$$d\mathrm{U}/\mathrm{a} = -d\rho/\rho \tag{1}$$

$$\mathrm{a}^2 = d\mathrm{P}/d\rho \tag{2}$$

where P and a are pressure and speed of sound, respectively. Applying the definition of speed of sound to a boundary cell, we find a relation between the density and pressure at the outlet as follows

$$\rho_{\mathrm{j,out}}{}^{\mathrm{new}} = \rho_{\mathrm{j,out}}{}^{\mathrm{old}} + \left(\mathrm{P_{out}} - \mathrm{P_{j,out}}\right)/\mathrm{a}^2_{\mathrm{j,out}} \tag{3}$$

Subscript *out* denotes values at channel outlet boundary. The *old* and *new* superscripts are corresponding to the values at previous and present time steps. Once the density is calculated, outlet temperature $\mathrm{T_{j,out}}$ at the cell j-th can be obtained from the equation of state

$$\mathrm{T_{j,out}} = \mathrm{P_{out}}/\left(\rho_{\mathrm{j,out}}\mathrm{R}\right) \tag{4}$$

where *R* is the gas constant. The velocity is also computed from the characteristic wave equation, obtained from multiplying Eq. (1) by speed of sound (a) and substituting definition of a^2 from Eq. (2) in the resulting equation. It yields

$$\mathrm{U_{j,out}}{}^{\mathrm{new}} = \mathrm{U_{j,out}}{}^{\mathrm{old}} + \left(\mathrm{P_{j,out}}\text{-}\mathrm{P_{out}}\right)/\left(\rho_{\mathrm{j,out}}\mathrm{a_{j,out}}\right) \tag{5}$$

Subscript *in* denotes values at channel inlet boundary. The inlet velocity is also calculated in the same way, as follows

$$\mathrm{U_{j,in}}{}^{\mathrm{new}} = \mathrm{U_{j,in}}{}^{\mathrm{old}} + \left(\mathrm{P_{in}}\text{-}\mathrm{P_{j,in}}\right)/\left(\rho_{\mathrm{j,in}}\mathrm{a_{j,in}}\right) \tag{6}$$

In addition, the density at the inlet is calculated from the equation of state

$$\rho_{\mathrm{j,in}} = \mathrm{P_{in}}/\left(\mathrm{T_{j,in}}\mathrm{R}\right) \tag{7}$$

Even though Eqs. (1) and (2) describe a wave in the continuum limit, their use in the DSMC simulation of rarefied flow is justified. In fact, DSMC algorithm assumes an equilibrium Maxwellian distribution for the particles which are injected into the flow field from inlet/outlet boundaries, as these particles come from free atmosphere [4, 28, 29]. From molecular gas dynamics, the Maxwellian distribution represents equilibrium condition, which could be described by Euler equations. As a result, application of wave equations, Eqs. (1) and (2), is approved. Suitable accuracy of the above equations in the simulation of internal micro/nano rarefied flows also confirms the use of aforementioned equations [21-23, 25, 26, 28, 29]. In our DSMC solver, the above equations are called at the end of "Enter" function, which computes the properties of incoming particles to the computational domain. Consequently, the estimated values of density, velocity, temperature and number of inserted particles in the inlet/outlet cells are corrected through Eqs. (3)-(7). At the steady state condition, the corrections to the old values are zero in Eqs. (3), (5), and (6). Thus, there is no

change in the hydrodynamics and thermal properties of gas flows at the inlet/outlet cells and correct values are applied.

3. Solver Verification

In this section we verify our DSMC solver. It should be reminded that our DSMC solver has been optimized by different features. The cell dimensions are chosen less than mean free path, i.e., smaller than $\lambda/3$ [30-33]. This criterion is implemented based on the local mean free path of cells. Each cell is subsequently divided into two sub-cells in each direction. The time step must be a fraction of the mean collision time and satisfy a Courant–Friedrichs–Lewy (CFL) number, based on the most probable molecular speed V_{mp}, less than one. Hadjiconstantinou [33] showed that the DSMC error exhibits quadratic dependence on the time step, and that for time steps of the order of one mean free time the error is of the order of 5%. According to mentioned criteria, we choose the time step equal to 0.08 of the minimum mean free time of all cells. Numbers of simulated particles are chosen such that there would be at least 20 particles in each cell [34]. Sampling of results starts as soon as the flow reaches to the steady state conditions. Flow sampling continues in sufficiently large time step intervals. In the beginning of the flow sampling period, flow properties set to zero and recalculated during the new sampling period. Using this process, the effects of initial unsteady results will be eliminated and convergence of the final flow properties could be traced.

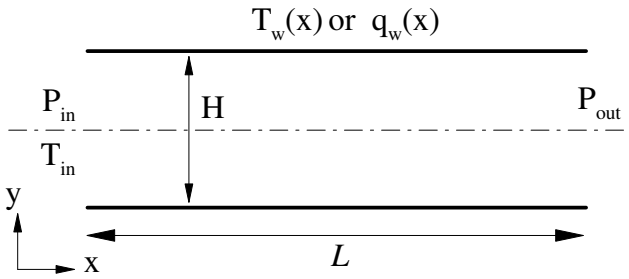

Figure 1. Micro/nanochannel geometry and imposed boundary conditions.

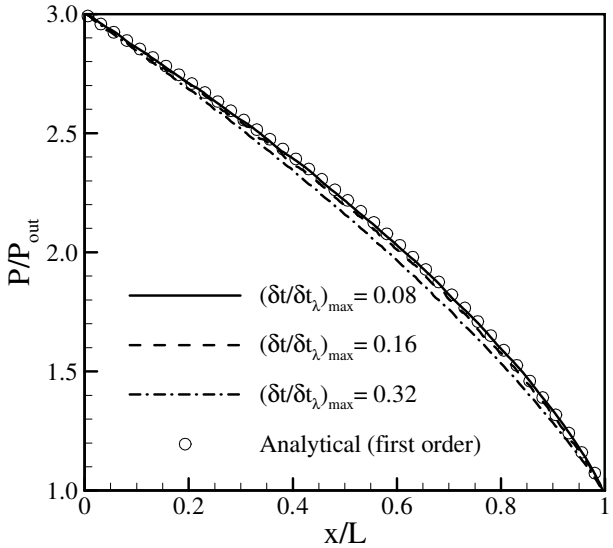

Figure 2. Pressure distribution along the channel for various DSMC time step values.

We evaluate our DSMC solver by solving subsonic pressure-driven nitrogen flow through microchannel imposing constant wall temperature condition. Channel length and height are 20 μm and 1 μm, respectively. Gas flow enters at the condition of $T_{in} = 300\,K, P_{in} = 4\,atm$. The channel pressure

ratio is set to 3 and channel walls have a uniform temperature distribution equal to 300 K. Geometry of the channel and imposed boundary conditions are shown in Figure 1. Figure 2 shows the effect of the DSMC time step on the pressure distribution along the channel. The results are compared with the analytical solution based on the first-order wall slip boundary condition given by [35]:

$$\frac{P}{P_{out}} = -6Kn_{Out} + \sqrt{\left(6Kn_{Out}\right)^2 + \left(1+12Kn_{Out}\right)\frac{x}{L} + \left(\Pi^2 + 12Kn_{Out}\Pi\right)\left(1-\frac{x}{L}\right)} \tag{8}$$

Eq. (8) presents streamwise distribution of normalized pressure along the channel based on the outlet Knudsen number (Kn_{Out}), channel pressure ratio (Π), channel length (L), and streamwise location (x). Lines in Figure 2 correspond to DSMC times steps equal to 0.08, 0.16, and 0.32 mean free time, respectively. Knudsen number ranges from 0.013 to 0.040 along the channel. According to Fig. 2, expect the large disagreements in the case of $\left(\delta t/\delta t_{\lambda}\right)_{max} = 0.32$, other values of specified time step well predict pressure distribution along the channel.

4. Thermal-Pressure-Driven Gas Flows

Thermal creep flow is an induced flow from the cold region towards the hot one. Thermal creep effect occurs only in the transitional rarefied flows, primarily along walls with a superimposed wall surface temperature gradient, see Figure 3.

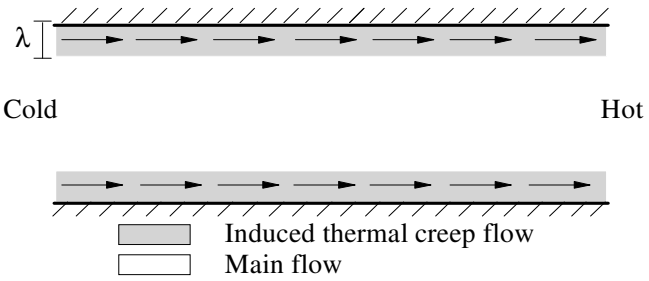

Figure 3. Thermal creep flow induced by wall temperature gradients.

For free molecular flows, thermal creep layer fills the entire channel, creating thermal transpiration flow. Meanwhile, in the case of transitional flow, the thermal creep effects are limited to the regions near the channel's wall [8]. At this stage, we consider the effect of thermal creep effect on the mass flow rate of Poiseuille flow. To achieve this, we simulate pressure-driven flows through channels with linear wall temperature distribution. To count the effects of flow rarefaction, we launch our study under different Knudsen numbers. Mass flow rate through micro/nano channels contains two parts as below:

$$\dot{m} = \dot{m}_p + \dot{m}_{th} \tag{9}$$

where subscript "p" corresponds to fully pressure-driven isothermal flow and subscripts "th" represents mass flow rate increment due to thermal creep effects. Thermal creep leads to an induced flow from the cold region to the hot one [36]. Therefore, streamwise wall temperature gradient increases mass flow rate and vice versa.

Figure 4 shows the effect of wall temperature gradient values on the thermal mass flow rate values. The results are obtained under different flow rarefaction conditions and streamwise wall temperature gradients. Figure 4(a) and (b) correspond to the bulk flow average temperature values of 300 K and 400 K, respectively. The x-component is wall temperature gradient in K, and X is the non-dimensional streamwise location, x/L, along the channel. According to the results, thermal mass flow rate increases linearly as wall temperature gradient increases for both average temperatures values.

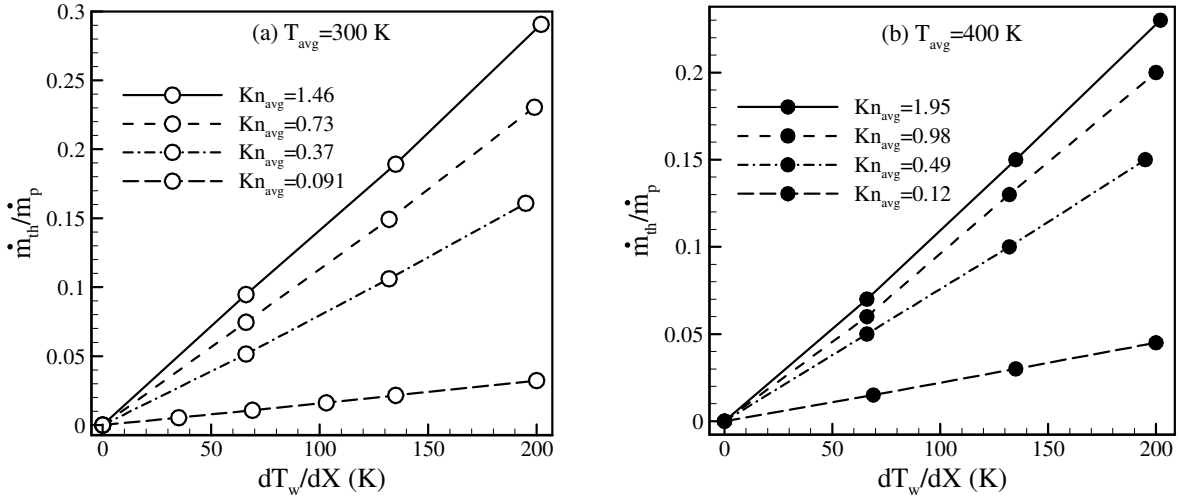

Figure 4. Non-dimensional thermal mass flow rate as a function of wall temperature gradient at different Knudsen numbers.

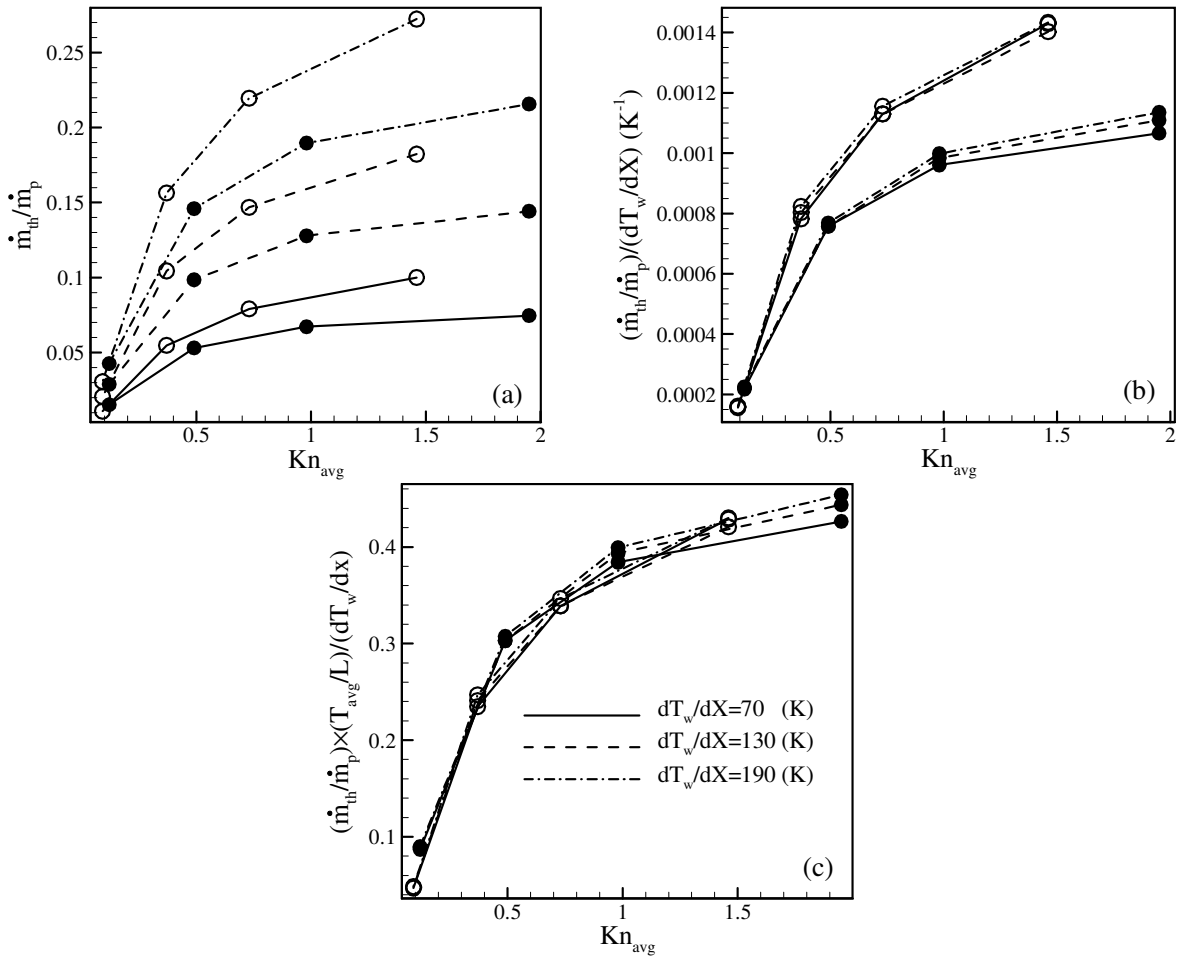

Figure 5. Thermal mass flow rate as a function of flow average Knudsen number, a) non-dimensional thermal mass flow rate, b) non-dimensional thermal mass flow rate independent from wall temperature gradient values, and c) non-dimensional thermal mass flow rate independent from wall temperature gradient and bulk flow temperature values. (White and black symbols denotes T_{avg} = 300 and 400 K, respectively)

The value of $\dot{m}_p$ is constant through variation of the wall temperature gradient and its value corresponds to the pure pressure-driven flow at zero wall temperature gradient condition. Figure 4 shows that increase in the thermal mass flow rate due to wall temperature gradient is faster for higher Knudsen numbers flows. It is also desired to study the thermal mass flow rate behavior with variation of the Knudsen number. For this aim, we have plotted the non-dimensional mass flux as a function of Knudsen number in Figure 5. Figure 5(a) shows the non-dimensional thermal mass flow rate as a function of the average Knudsen number at different wall temperature gradient values, i.e., 70 K, 130 K, and 190 K. White and black symbols correspond to the average flow temperature values of 300 K and 400 K, respectively. According to Figure 5(a), at a specified wall temperature gradient value, thermal mass flow rate increases as flow's average Knudsen number increases. The rate of increase is faster at lower Knudsen numbers and higher wall temperature gradient values. To make the results independent from the wall temperature gradient values, we normalize the results of Figure 5(a) by the wall temperature gradient values. This is shown in Figure 5(b). As it seen in Figure 5(b), the results for both average temperature values of 300 K (white) and 400 K (black) have the same trend versus the flow Knudsen umber. Therefore, we normalize graphs of Figure 5(b) to their average temperature values. It leads to Figure 5(c). It is well seen that both lines of Figure 5(b) have the same trend in Figure 5(c).

Actually the results given in Figure 5(c) are independent from the average flow temperature and wall temperature gradient values. According to Figure 5(c), at a specified wall temperature gradient and average flow temperature values, thermal mass flow rate increases as the flow rarefaction increases. This increase is slower at higher Knudsen number regimes. We extend the results given in Figure 5(c) to the free molecular regime to obtain a reliable correlation formula for prediction of the thermal mass flow rate at all ranges of the Knudsen number. As already stated, we produce higher values of flow rarefaction by reducing channel inlet/outlet pressure values. We have performed a large set of DSMC simulations in the third part of our investigations under different conditions of flow average temperature, rarefaction, and wall temperatures. An inlet pressure of 0.15 atm with a pressure ratio of 2 is considered.

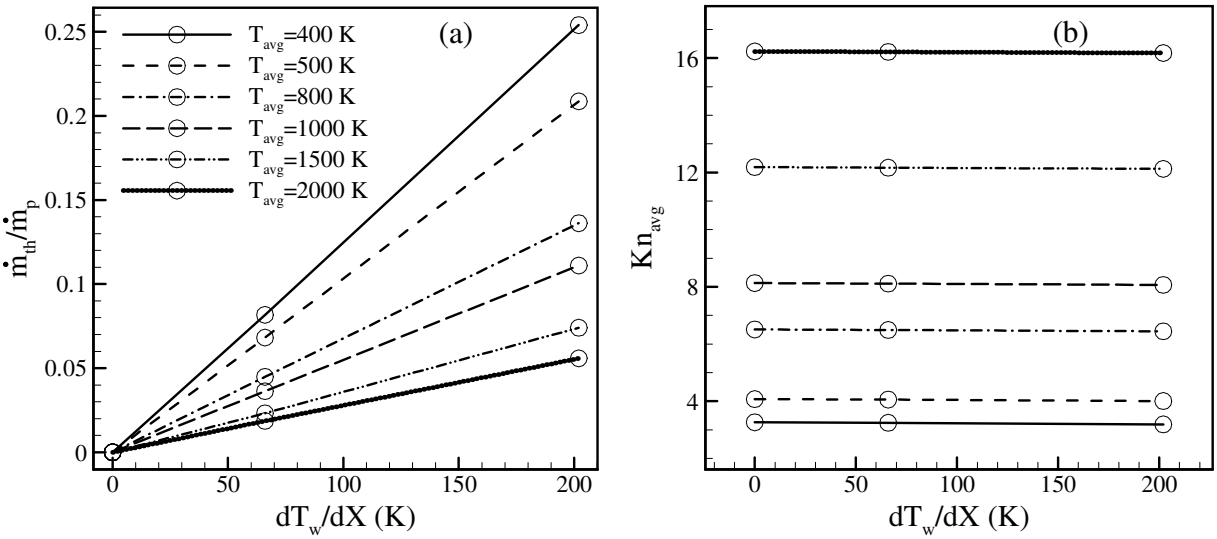

Figure 6. Thermal creep effects at high flow rarefaction and different flow temperature values; a) thermal mass flow rate and b) average Knudsen number.

Figure 6(a) shows the mass flow increments due to the wall temperature gradients under different values of the average flow temperature at higher values of Knudsen number. There is a linear correlation between the thermal mass flow rate and wall temperature gradient similar to that given of

in Figure 4. Figure 6(b) plots the average flow Knudsen numbers for different values of T_{avg}. Each line corresponds to the same inlet/outlet boundary condition values, but symbols on each line are related to different linear wall temperature distributions. According to Figure 6(b), average Knudsen number is approximately constant on each line. It is because wall temperature was changed in such a way that average wall temperature is fixed to the desired T_{avg} value. This permitted us to study thermal creep effects only under different wall temperature gradient values at constant flow rarefaction.

We made a trend study for results of Figure 6 similar to what is performed in Figure 5. The results are plotted for all ranges of Knudsen number in Fig. 7. According to the Figure 7, we could cross a correlated line which contains the effects of flow rarefaction, average temperature, wall temperature gradient, and channel pressure ratio on the thermal mass flow rate increment of the Poiseuille flow. The resulting correlated line shows that the increase in the "non-dimensional thermal mass flow rate" slows down as the Knudsen number increases and reaches to a constant magnitude in the free molecular region. According to the Fig. 7, non-dimensional thermal mass flow rate increases from zero (in the case of continuum flow) to a limiting value of 0.578 at the free molecular regime. The results represents that thermal mass flow rate has a linear dependency on the wall temperature gradient value at the free molecular region. It also shows that the thermal mass flow rate increases as the flow rarefaction increases.

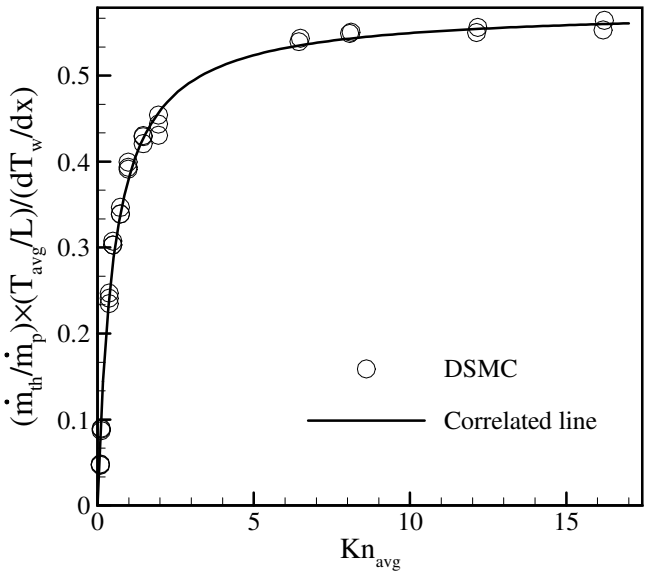

Figure 7. Thermal mass flow rate versus flow rarefaction from slip to free molecular regime.

5. Conclusion

We present a mass flow ate study for simultaneous thermal-pressure-driven flows through micro-/nanoscale channels using an improved DSMC solver. Thermal-driven forces were generated by non-uniform wall temperature distribution. The effects of thermal creep studied over a wide range of flow rarefaction from the slip to free molecular regime. We showed that thermal mass flow rate linearly increases as wall temperature gradient increases. The effect of wall temperature gradient is stronger at lower bulk temperature values. We presented a non-dimensional thermal mass flow rate which is just depends on the average flow Knudsen number. Our results showed that the non-dimensional thermal creep mass flow rate increment of the Poiseuille flow increases as flow rarefaction increases and it approaches to value of 0.578 at the free molecular limit. The obtained results would be useful in the mass flow rate prediction of Poiseuille flow under specific wall heat flux conditions.

References

[1] J. Taylor and C. L. Ren, "Application continuum mechanics to fluid flow in nanochannels," Microfluid. Nanofluid. **1** (4), 356 (2005).
[2] C. M. Ho and Y. C. Tai, "Micro-electro-mechanical-system (MEMS) and fluid flows," Annu. Rev. Fluid Mech. **30**, 579 (1998).
[3] C. Cercignani, *The Boltzmann equation and its applications* (Springer, New York, 1987).
[4] G. A. Bird, *Molecular Gas Dynamics and the Direct Simulation of Gas Flows* (Oxford Science, Oxford, 1994).
[5] Y. Sone, *Kinetic Theory and Fluid Dynamics* (Birkhäuser, Boston, 2002).
[6] Y. Sone, Y. Waniguchi, and K. Aoki, "One-way flow of a rarefied gas induced in a channel with a periodic temperature distribution," Phys. Fluids **8** (8), 2227 (1996).
[7] A. A. Alexeenko, S. F. Gimelshein, E. P. Muntz, and A. D. Ketsdever, "Kinetic modeling of temperature driven flows in short microchannels," Int. J. Thermal Sci. **45**, 1045 (2006).
[8] Y.-L. Hana, E. P. Muntza, A. Alexeenkob, and M. Young, "Experimental and computational studies of temperature gradient-driven molecular transport in gas flows through nano/microscale Channels," Nanoscale Microscale Thermophys. Eng. **11**, 151 (2007).
[9] Y. L. Han, "Thermal-creep-driven flows in Knudsen compressors and related nano/microscale gas transport channels," J. Microelectromech. Syst. 17 (4), 984-997 (2008).
[10] S. K. Loyalka, "Kinetic theory of thermal transpiration and mechanocaloric effect. I," J. Chem. Phys. **55** (9), 4497 (1971).
[11] S. K. Loyalka, "Slip in the thermal creep flow," Phys. Fluids **14** (1), 21 (1971).
[12] S. K. Loyalka, "Kinetic theory of thermal transpiration and mechanocaloric effect. II," J. Chem. Phys. **63** (9), 4054 (1975).
[13] S. K. Loyalka and T. S. Storvick, "Kinetic theory of thermal transpiration and mechanocaloric effect. III. Flow of a polyatomic gas between parallel plates," J. Chem. Phys. **71** (1), 339 (1979).
[14] S. S. Lo, S. K. Loyalka, and T. S. Storvick, "Kinetic theory of thermal transpiration and mechanocalorlc effect. V. Flow of polyatomic gases in a cylindrical tube with arbitrary accommodation at the surface," J. Chem. Phys. **81** (5), 2439 (1984).
[15] T. Kanki and S. Iuchi, "Poiseuille fllow and thermal creep of a rarefied gas between parallel plates," Phys. Fluids **16** (5), 594 (1973).
[16] T. Ohwada, Y. Sone, and K. Aoki, "Numerical analysis of the Poiseuille and thermal transpiration flows between two parallel plates on the basis of the Boltzmann equation for hard-sphere molecules," Phys. Fluids A **1** (12), 2042 (1989).
[17] P. Taheri and H. Struchtrup, "Rarefaction effects in thermally-driven microflows," Physica A **389**, 3069 (2010).
[18] M. A. Gallis, J. R. Torczynski, D. J. Rader, and G. A. Bird, "Convergence behavior of a new DSMC algorithm," J. Comput. Phys. **228**, 4532 (2009).
[19] S. Stefanov, "Particle Monte Carlo algorithms with small number of particles in grid cells, in Numerical Methods and Applications," Lecture Notes in Comput. Sci. **6064**, 110 (2010).
[20] S. Stefanov, "On DSMC calculations of rarefied gas flows with small number of particles in cells," SIAM J. Sci. Comput. **33**, 677 (2011).
[21] E. Roohi and M. Darbandi, "Extending the Navier–Stokes solutions to transition regime in two-dimensional micro- and nanochannel flows using information preservation scheme," Phys. Fluids **21** (2009).
[22] E. Roohi, M. Darbandi, and V. Mirjalili, "Direct Simulation Monte Carlo Solution of Subsonic Flow through Micro/Nanoscale Channels," Journal of Heat Transfer **131**, 92402 (2009).

[23] M. Darbandi and E. Roohi, "Study of Subsonic/supersonic Gas Flow through Micro/nanoscale Nozzles Using Unstructured DSMC Solver," Microfluidics and Nanofluidics **10**, 321 (2011).
[24] T. J. Scanlon, E. Roohi, C. White, M. Darbandi, and J. M. Reese, "An open source, parallel DSMC code for rarefied gas flows in arbitrary geometries," Computers & Fluids **39**, 2078 (2010).
[25] E. Roohi and M. Darbandi, "Recommendations on Performance of Parallel DSMC Algorithm in Solving Subsonic Nanoflows," Applied Mathematical Modeling **36**, pp. 2314-2321, (2012).
[26] M. Darbandi and E. Roohi, "DSMC Simulation of Subsonic Flow through Nanochannels and Micro/Nano Steps," International Communication in Heat and Mass Transfer, **38** (10), pp. 1444-1449, (2011).
[27] O. Ejtehadi, E. Roohi, and J. Abolfazli, "Investigation of Basic Molecular Gas Structure Effects on Hydrodynamics and Thermal Behaviors of Rarefied Shear Driven Flow Using DSMC", International Communication in Heat and Mass Transfer, **39** (3), pp. 439-448, (2012).
[28] W. Liou and Y. Fang, "Implicit Boundary Conditions for Direct Simulation Monte Carlo Method in MEMS Flow Predictions," Computer Modeling in Engineering & Science **1**, 119 (2000).
[29] M. Wang and Z. Li, "Simulations for gas flows in Microgeometries using the direct simulation Monte Carlo method," International Journal of Heat and Fluid Flow **25**, 975 (2004).
[30] F. J. Alexander, A. L. Garcia, and B. J. Alde, "Cell size dependence of transport coefficients in stochastic particle algorithms," Phys. Fluids **10** (6), 1540 (1998).
[31] F. J. Alexander, A. L. Garcia, and B. J. Alder, "Erratum: ``Cell size dependence of transport coefficients in stochastic particle algorithms" [Phys. Fluids [bold 10], 1540 (1998)]," Physics of Fluids **12** (3), 731 (2000).
[32] Z. X. Sun, Z. Tang, Y. L. He, and W. Q. Tao, "Proper cell dimension and number of particles per cell for DSMC," Computers & Fluids (2011).
[33] N. G. Hadjiconstantinou, "Analysis of discretization in the direct simulation Monte Carlo," Phys. Fluids **12** (10), 2634 (2000).
[34] C. Shu, X. H. Mao, and Y. T. Chew, "Particle number per cell and scaling factor effect on accuracy of DSMC simulation of micro flows," Int. J. Numer. Methods Fluids **15** (8), 827 (2005).
[35] E. B. Arkilic, M. A. Schmidt, and K. S. Breuer, "Gaseous slip flow in long microchannels," J. Microelectromech. Syst. **6** (2), 167 (1997).
[36] G. E. Karniadakis, A. Beskok, and N. Aluru, *Microflows and Nanoflows: Fundamentals and Simulation* (Springer-Verlag, New York, 2005).